DOI 10.1007/s10812-025-01967-1
Journal of Applied Spectroscopy, Vol. 92, No. 4, September, 2025 (Russian Original Vol. 92, No. 4, July–August, 2025)

SURFACE MORPHOLOGY, OPTICAL CHARACTERISTICS AND ELECTROPHYSICAL PROPERTIES OF Nb_2O_5 FILMS

N. A. Bosak,[a,*] P. V. Shpak,[a] A. N. Chumakov,[a] L. V. Baran,[b] V. V. Malutina-Bronskaya,[c] V. S. Drobush,[a] and A. S. Kuzmitskaya[c]

UDC 621.323.826:(533.9+537.9)

Results are given for a complex study of thin Nb_2O_5 films deposited in vacuum (p = 2.2 Pa) on quartz and silicon substrates using multi-pulse high-frequency laser action (f ~ 10–12 kHz) on a ceramic target with laser power density q = 81 MW/cm^2. The morphology of these films was studied using atomic force microscopy. Features of the transmission spectra were presented. The photoelectrical properties of the Nb_2O_5/Si structure were analyzed.

Keywords: *high-frequency laser action, thin film, transmission and reflection spectra, current–voltage and farad–voltage characteristics, spectral sensitivity.*

Introduction. Nanostructured metal oxide films are commonly used in microelectronics [1, 2]. Niobium oxide (Nb_2O_5) holds considerable promise for use as a material for electrical and optical applications with exceptional properties such as a high refraction index ($n = 2.4$ at $\lambda = 550$ nm), high dielectric permeability, stability in air and water, resistance to acids and bases, low absorption and high transparency in the UV and visible ranges as well as in the near-IR region from 380 nm to 9 μm [3]. Niobium oxide is a commonly used alternative to TiO_2, which absorbs radiation with $\lambda < 400$ nm. Thin Nb_2O_5 films are excellent materials for use in a wide variety of new applications in microelectronics, including optical [4] and solar elements [5], optical UV filters, protective optical coatings, electrochromic devices, chemical sensors [6], photoelectrodes, high energy density condensers, and shutters [7–9].

Thin Nb_2O_5 films can be obtained by various procedures including DC/RF plasma magnetronic spraying, ion beam spraying (IBS), electron beam evaporation, thermal oxidation, photochemical deposition from the gas phase, plasma-enhanced chemical vapor deposition (PECVD), spray pyrolysis, sol-gel methods, and pulse laser deposition (PLD) [10–17]. Nb_2O_5/Si photodiode structures obtained by chemical methods have been studied by Georgiev et al. [18] and Salim et al. [19, 20]. The photosensitivity of the Nb_2O_5/Si structure depends on the method of preparation and type of conductivity of the silicon substrate. Thus, the study of nanostructured thin Nb_2O_5 films holds importance for their possible application in photodetectors [21].

In the present work, we studied the structural, optical, and photoelectric properties of thin Nb_2O_5 films obtained by multi-pulse high-frequency laser deposition in vacuum onto quartz and silicon substrates [22].

Experiment. Thin Nb_2O_5 films were obtained by high-frequency laser deposition onto a ceramic target in vacuum ($p = 2.2$ Pa). The experimental laser apparatus with controlled pulse repetition frequency from 5 to 50 kHz consisted of a laser radiation source with wavelength $\lambda = 1.06$ μm, an optical system for conveying the laser radiation to the sprayed target, a vacuum chamber, and measurement module. The laser pulse repetition frequency was changed by varying the level of laser pumping and the optical density of the shutter consisting of irradiated crystalline lithium fluoride with F_2^- color sites. The duration of the laser pulses at half-height τ was about 85 ns. The deposition of the microscopically homogeneous thin films was carried out with laser radiation power density $q = 81$ MW/cm^2 and pulse repetition frequency $f \sim 10$–12 kHz.

[*] To whom correspondence should be addressed.

[a] B. I. Stepanov Institute of Physics, National Academy of Sciences of Belarus, Minsk, Belarus; email: n.bosak@ifanbel.bas-net.by; [b] Belarusian State University, Minsk, Belarus; email: baran@bsu.by, [c] SSPA "Optics, Optoelectronics, and Laser Technology," Minsk, Belarus; email: malyutina@oelt.basnet.by. Translated from Zhurnal Prikladnoi Spektroskopii, Vol. 92, No. 4, pp. 462–468, July–August, 2025. Original article submitted March 13, 2025, final version received March 31, 2025; accepted for publication April 25, 2025.

The surface morphology of the samples was studied using an NT-MDT Spectrum Solver P47-Pro scanning probe microscope (manufactured in Russia) in semicontact mode. We used super-sharp contacless whisker-type silicon cantilevers with probe circumferential radius <3 nm. The thickness of the Nb_2O_5 film measured by atomic force microscopy (AFM) was ~100 nm. The major roughness parameters were determined at five different points on the sample upon scanning a 20 × 20-μm region. The optical radiation transmission of the thin films in the near-IR spectral region was recorded using a Thermo Nicolet Nexus Fourier-transform IR spectrometer at 400–4000 cm^{-1}.

The transverse current–voltage characteristics (CVC) of the Nb_2O_5/Si structures were measured with an automated standard test laser complex using a multi-spectral source of laser radiation (set of laser diodes with λ = 405, 450, 520, 660, 780, 808, 905, 980, and 1064 nm) with a common optical fiber outlet and calibrated radiation power of ~2 mW. The CVC were measured without the action of laser radiation and with laser action at different wavelengths. The farad–voltage characteristics (FVC) were measured using an E7-20 RLC immitance meter at signal frequencies 100 kHz and 1 MHz, including by the action of laser radiation with λ = 520, 660, and 808 nm. All the measurements were carried out at room temperature. A tungsten probe was selected as the upper electrode on the Nb_2O_5 film. InGa eutectic paste was used for contact of the silicon substrate with the measurement unit (lower electrode).

Results and Discussion. AFM images of the surface morphology of the Nb_2O_5 films deposited by high-frequency laser spraying of an oxide ceramic in vacuum onto a quartz substrate are presented in Fig. 1. Atomic force microscopy showed that the deposition onto the quartz substrate gives a smooth homogeneous film surface with mean height difference of 10 nm and root mean-square roughness of 4 nm. Homogeneously arranged particles with density 2 particles/μm^2 are seen on the film surface. The transverse particle size distribution histograms (Fig. 1c) and cross-section profile along the selected line (Fig. 1d) show that the mean lateral particle length is 70 nm and the particle height is 20–30 nm.

Figure 2 gives the AFM images of the surface morphology of the Nb_2O_5 films deposited onto a silicon substrate. The deposition onto the silicon substrate gives a smooth homogeneous film surface with mean height difference 21 nm and root mean-square roughness of 8 nm. Homogeneously arranged dendrites with branch length 0.5–2.5 μm and height ≤25 nm were found over the entire film surface.

The transmission (T) of our laser-deposited Nb_2O_5 film on a quartz substrate in the near-IR spectral region shown in Fig. 3a increases from 2% at λ = 1000 nm to 22% at λ = 2580 nm. The transmission of the unsprayed quartz substrate T = 91% in the broad spectral region from λ = 424 nm to 1728 nm. The transmission of the Nb_2O_5 film in the medium IR region rises sharply from T = 0.6% at frequency ν = 3600 cm^{-1} to T = 34% at ν = 3880 cm^{-1} (Fig. 3b). In the reflection spectrum, R for the Nb_2O_5 film on a quartz substrate drops from R = 22.7% at λ = 189 nm to the minimal value R = 13.4% at λ = 384 nm and then increases to R = 19.% at λ = 1013 nm.

The transmission of silicon (1) and of laser-deposited Nb_2O_5 film on a silicon substrate shown in Fig. 4a increases sharply from T = 1.4% at λ = 997 nm to T = 32% at λ = 1200 nm followed by a smooth increase to T = 60% at λ = 2980 nm. The transmission of the Nb_2O_5 film in the medium IR region increases from T = 22.8% at frequency ν = 403 cm^{-1} to T = 66.9% at ν = 2447 cm^{-1} and then gradually decreases to T = 58.6% at frequency ν = 3880 cm^{-1} (Fig. 4b). Interference is observed in the broad frequency range 653–3297 cm^{-1} due to the thin Nb_2O_5 film. In the reflection spectrum, we find a drop in the R value of the Nb_2O_5 film on a silicon substrate (Fig. 4c) from R = 30.4% at λ = 192 nm to a minimal value of R = 14.4% at λ = 368 nm as well as five maxima at λ_1 = 288 nm, λ_2 = 330 nm, λ_3 = 407 nm, λ_4 = 560 nm, and λ_5 = 902 nm.

The measurements of the FVC were carried out for a qualitative evaluation of the separation boundary of the structure. The measured high-frequency FVC at signal frequencies 100 kHz and 1 MHz have a shape typical of MOSFET structures. At signal frequency 100 kHz, we observed dependence of the FVC on the wavelength of the operating radiation. The finding of hysteresis in the FVC and its decreasing magnitude with increasing frequency of the measurement signal can be related to the existence of an embedded charge due to the presence of rapid surface states on the separation boundary and in the oxide including those related to the presence of dendrites. The existence of a maximum in the region of FVC capacitance modulation (signal frequency 1 MHz) from 0 to 4 V indicates an intermediate nonstoichiometric silicon oxide. Figure 5a shows the FVC of the Nb_2O_5 structure measured at signal frequency 1 MHz without irradiation and with laser irradiation at λ = 808 nm. The transition capacitance decreases with increasing reverse voltage. This result is attributed to an increase in the width of the depleted region with bias voltage. The existence of maxima and hysteresis in the region of capacitance modulation (at voltages from 0 to +20 V) indicates the presence of surface states on the separation boundary of the Nb_2O_5/Si structure, which participate in the charge transfer process. Since the specific resistance in an oxide film is higher than for the silicon substrate, the leakage current through the Nb_2O_5/Si structure in the voltage region, corresponding

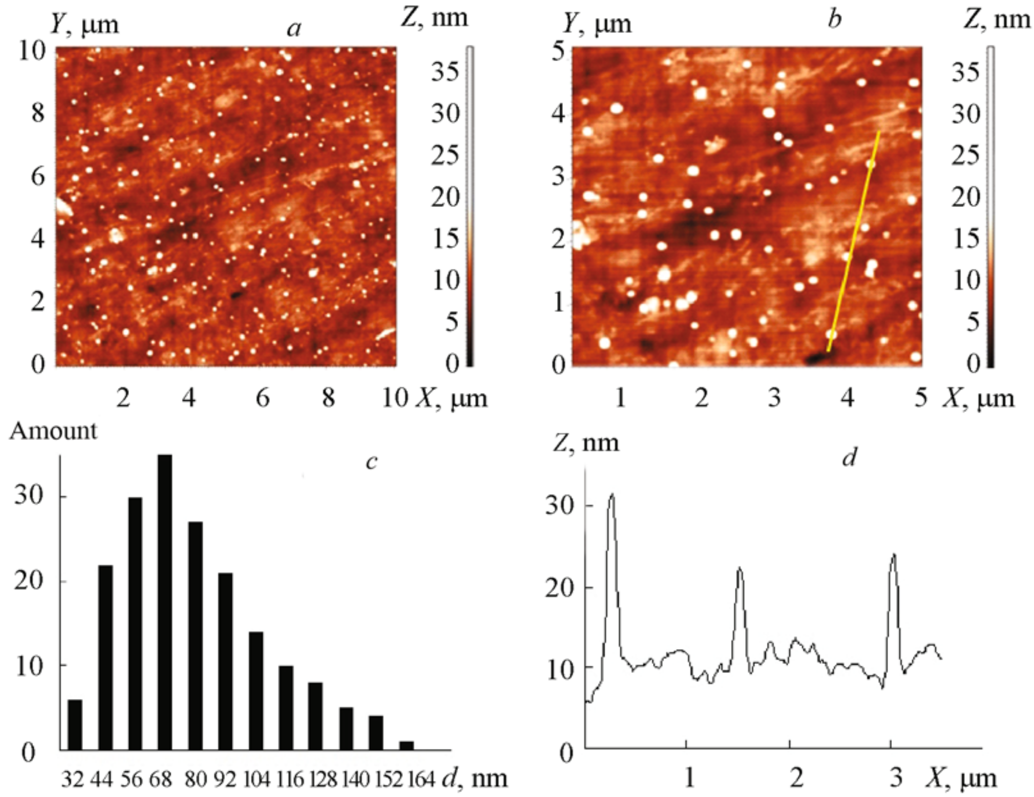

Fig. 1. Surface morphology of an Nb_2O_5 film on a quartz substrate: a, b) two-dimensional AFM image, c) histogram for the lateral particle length distribution, d) profile along the cross section along the selected line in Fig. 1b.

to enrichment of the semiconductor surface region, is a function of the resistance of the oxide film. The decrease in the capacitance in the region of negative voltages upon laser irradiation occurs because the rate of generation of free carriers is lower than the rate of their leakage through the Nb_2O_5/Si separation boundary [23]. The existence of an intermediate layer of nonstoichiometric silicon oxide and surface states can also account for the photosensitivity of FVC in the IR region at $\lambda = 808$ nm.

Figure 5b shows the CVC of the Nb_2O_5/*p*-Si structure. The dark CVC have virtually symmetric shape. At bias voltage less than +12 V, we observe a recombination current since the generated electron–hole pairs recombine and do not contribute to the overall current. When the bias voltage is greater than +12 V, there is a rapid exponential increase in the current with increasing applied voltage, which corresponds to a diffusion current. The reverse current increases with increasing applied voltage, which suggests the existence of defects on the surface of the separation boundary of the Nb_2O_5/Si structure. For the Nb_2O_5/*p*-Si heterojunction, the barrier decreases upon forward bias (e.g., reverse bias applied onto the Nb_2O_5 film) with increasing applied bias and the current begins to increase rapidly. In the case of the reverse bias of the junction, in contrast, the barrier increases and greater current is observed at voltages greater than 3 V [24]. A photoeffect is observed upon the action of laser irradiation in the region of negative voltages applied to the Nb_2O_5 film. The shape of the current–voltage curve for the Nb_2O_5/*p*-Si structure upon laser irradiation can be attributed to the existence of a broad depleted layer and a large length of diffusion of the nonbasic charge carriers in the *p*-type substrate such that the photons in this region are absorbed and the generated electron–hole pair separates with high efficiency, creating a photocurrent. The current–voltage measurements were used to calculate the spectral sensitivity of the Nb_2O_5/Si structure at bias voltage –20 V

$$S = (I_{ph} - I_d)/P_\lambda ,$$

where I_{ph} is the photocurrent induced by laser irradiation at wavelength λ, I_d is the dark current of the structure, and P_λ is the laser output at wavelength λ.

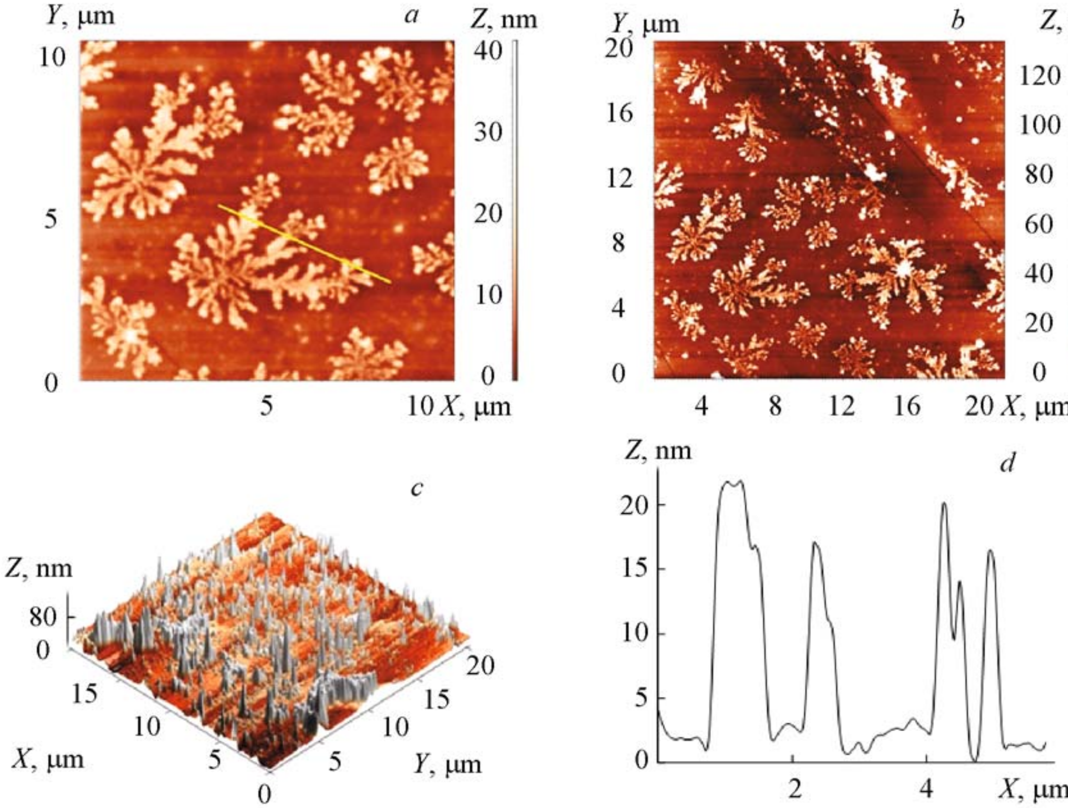

Fig. 2. Surface morphology of an Nb_2O_5 film on a silicon surface: a, b) two-dimensional AFM image, c) three-dimensional AFM image, d) profile of the cross section along the selected line in Fig. 2a.

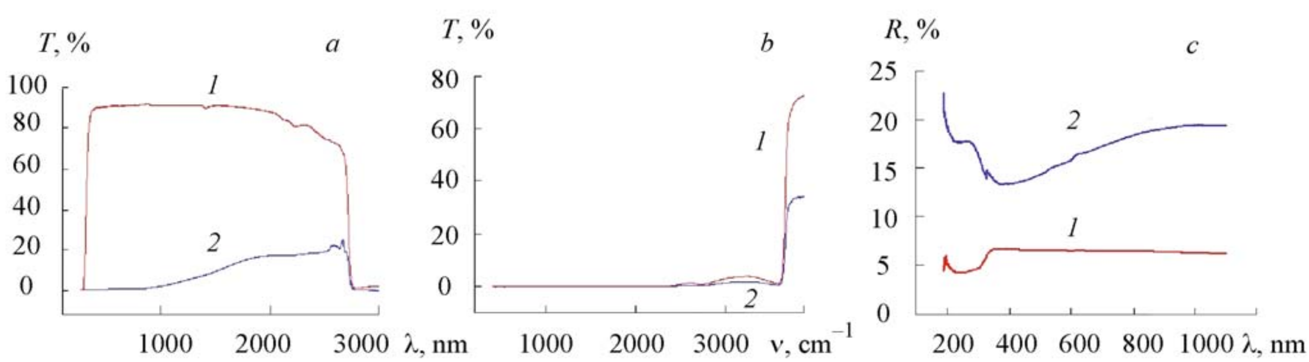

Fig. 3. Transmission spectra of quartz (1) and the laser-deposited Nb_2O_5 film on a quartz substrate (2) in the visible and near-IR (a) and medium IR regions (b); reflection spectra of quartz (1) and laser-deposited Nb_2O_5 film on a quartz substrate (2) in the visible and near-IR regions (c).

This gave the spectral sensitivity of the Nb_2O_5/*p*-Si structure at bias voltage –20 V (Fig. 5c). The plot for the spectral sensitivity of the Nb_2O_5/*p*-Si structure shows a maximum in the near-IR of ~66 mA/W at λ = 808 nm. The photosensitivity in the region λ < 660 nm can be a consequence of absorption in the thin Nb_2O_5 film and is related to the

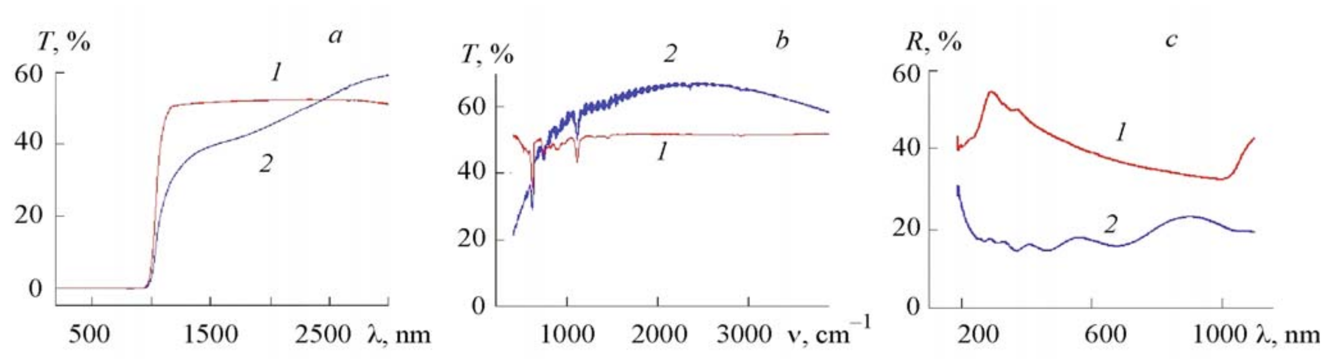

Fig. 4. Transmission spectra of silicon (1) and of a laser-deposited Nb_2O_5 film on a silicon substrate (2) in the visible and near-IR (a) and medium IR regions (b); reflection spectra of the silicon substrate (1) and of the laser-deposited Nb_2O_5 film on a silicon substrate (2) in the visible and near-IR regions (c).

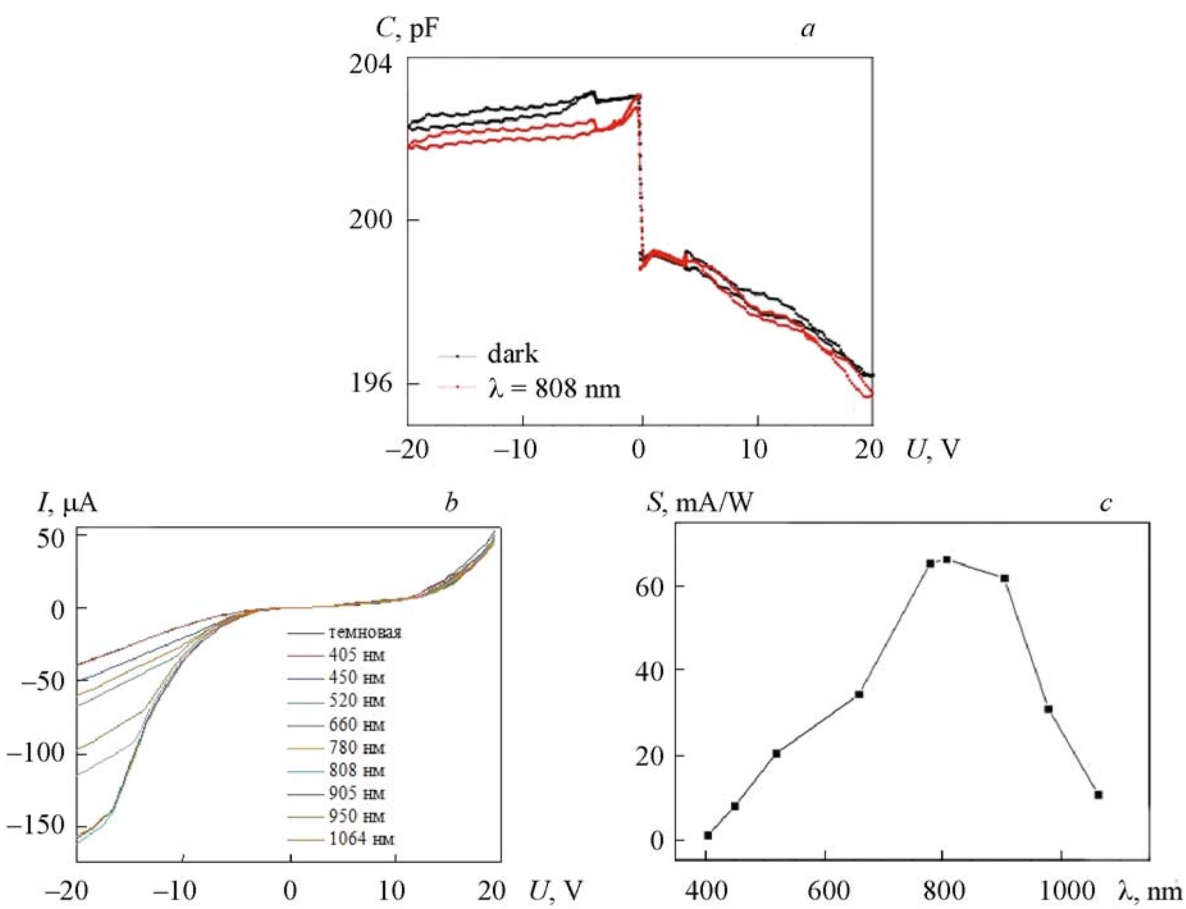

Fig. 5. Farad–voltage (a) and current–voltage characteristics (b) as well as the spectral sensitivity of the Nb_2O_5/Si structure at U = –20 V (c).

width of the band gap of the oxide. The high photosensitivity in the near-IR region may suggest that the photons absorbed by the silicon substrate are transformed into photocurrents more efficiently than photons absorbed by the thin oxide film [25].

Conclusions. High-frequency laser spraying was used to obtain nanostructured Nb_2O_5 films on silicon substrates with mean height difference 21 nm and root mean-square roughness 8 nm. Homogeneously arranged dendrites were found on the film surface. The transmission of the laser-deposited Nb_2O_5 film on a silicon substrate in the near-IR region sharply increases from 1.4% at λ = 997 nm to 32% at λ = 1200 nm, A photoeffect is induced by laser irradiation in the negative voltage region. The Nb_2O_5/*p*-Si structure upon forward bias of –20 V has photosensitivity to radiation with λ = 450–980 nm, while a sensitivity maximum at ~65 mA/W is observed in the near-IR region (808 nm), which suggests the feasibility of using these structures in photodetectors.

REFERENCES

1. E. Çetinögü-Goldenberg, J.-E. Klemberg-Sapieha, and L. Martinu, *Appl. Opt*., **51**, No. 27, 6498–6507 (2012).
2. A. V. Rosario and E. C. Pereira, *Sol. Energy Sol. Cells*, **71**, No. 1, 41–50 (2002).
3. C. C. Lee, C. L. Tien, and J. C. Hsu, *Appl. Opt.*, **41**, No. 10, 2043–2047 (2002).
4. B. Reichmann and A. J. Bard, *J. Electrochem. Soc.*, **127**, No. 1, 241–242 (1980).
5. J. B. Xia, N. Masaki, K. J. Jiang, and S. J. Yanagida, *Photochem. Photobiol. A: Chem.*, **188**, No. 1, 120–127 (2007).
6. M. E. Gimon-Kinsel and K. J. Balkus, Jr., *Microporous Mesoporous Mater.*, **28**, No. 1, 113–123 (1999).
7. F. Lai, M. Li, H. Wang, H. Hu, X. Wang, J. G. Hou, Y. Song, and Y. Jiang, *Thin Solid Films*, Nos. 1–2, 314–320 (2005).
8. Y. Zhao, X. Zhou. L. Ye, and S. Chi Edman Tsang, *Nano Rev.*, **3**, No. 1, 17631(1–11) (2012).
9. Y. Huang, Y. Xu, S.-J. Ding, H.-L. Lu, Q.-Q. Sun, D. W. Zhang, and Z. Chen, *Appl. Surf. Sci.*, **257**, No. 16, 7305–7309 (2011).
10. R. A. Rani, A. S. Zoolfakar, A. P. O'Mullane, M. W. Austin, and K. Kalantar-Zadeh, *J. Mater. Chem. A*, **2**, No. 38, 15683–15703 (2014).
11. N. C. Emeka, P. E. Imoisili, and T.-C. Jen, *Rev. Coat.*, **10**, No. 12, Article ID 1246(1–28) (2020).
12. R. Panetta, A. Latini, I. Pettiti, and C. Cavallo, *Mater. Chem. Phys.*, **202**, 289–301 (2017).
13. R. Chandrasekharan, I. Park, R. I. Masel, and M. A. Shannon, *J. Appl. Phys.*, **98**, No. 11, Article ID 114908 (2005).
14. J.-P. Masse, H. Szymanowski, O. Zabeida, A. Amassian, J. E. Klemberg-Sapieha, and L. Martinu, *Thin Solid Films*, **515**, No. 4, 1674–1682 (2006).
15. H. Szymanowski, O. Zabeida, J. E. Klemberg-Sapieha, and L. Martinu, *J. Vac. Sci. Technol. A: Vac., Surf., Film*, **23**, No. 2, 241–247 (2005).
16. S. H. Mujawar, A. I. Inamdar, S. B. Patil, and P. S. Patil, *Solid State Ionics*, **177**, Nos. 37–38, 3333–3338 (2006).
17. A, M. Al-Baradi, M. M. El-Nahass, A. M. Hussanien, A. A. Atta, M. S. Alqahtani, and A. O. Aldawsari, *Optik (Stuttg.)*, **168**, 853–863 (2018).
18. R. Georgiev, B. Georgieva, M. Vasileva, P. Ivanov, and T. Babeva, *Adv. Cond. Matter Phys.*, **2015**, Article ID 403196(1–8) (2015).
19. E. T. Salim and H. T. Halboos, *Mater. Res. Express*, **6**, No. 6, Article ID 066401 (2019).
20. M. Abood, E. T. Salim, and J. A. Saimon, *J. Ovonic Res.*, **15**, No. 2, 109–115 (2019).
21. E. T. Salim, J. A. Saimon, M. K. Abood, and M. A. Fakhri, *Opt. Quant. Electron.*, **52**, No. 10, 463 (2020).
22. A. N. Chumakov, V. B. Avramenko, and N. A. Bosak, *J. Appl. Spectrosc.*, **79**, No. 2, 261–268 (2012).
23. V. F. Kabanov, A. M. Sverdlova, and D. A. Korotkov, *Fiz. Tekhn. Poluprovodn.*, **30**, No. 10, 1756–1760 (1996).
24. C. Van Opdorp and H. K. J. Kanerva, *Solid State Electron.*, **10**, No. 5, 401–421 (1967).
25. M. J. Cristea, *Electron. Instrum. Eng. Int. J. (EEIEJ)*, **1**, No. 3, 29–38 (2014).